Fermilab FERMILAB-Pub-01/231-T August 2001

Chaos, ergodicity, and the thermodynamics of lower-dimensional time-independent Hamiltonian systems

Henry E. Kandrup*
Department of Astronomy, Department of Physics, and Institute for Fundamental Theory
University of Florida, Gainesville, Florida 32611

Ioannis V. Sideris†
Department of Astronomy, University of Florida, Gainesville, Florida 32611

C. L. Bohn‡
Fermilab, Batavia, Illinois 60510
(August 3, 2001)

This paper uses the assumptions of ergodicity and a microcanonical distribution to compute estimates of the largest Lyapunov exponents in lower-dimensional Hamiltonian systems. That the resulting estimates are in reasonable agreement with the actual values computed numerically corroborates the intuition that chaos in such systems can be understood as arising generically from a parametric instability and that this instability can be modeled by a stochastic-oscillator equation (*cf.* Casetti, Clementi, and Pettini, Phys. Rev. **E 54**, 5969 (1996)), linearised perturbations of a chaotic orbit satisfying a harmonic-oscillator equation with a randomly varying frequency.

PACS number(s): 05.45.+h, 02.40.-k, 05.20.-y

I. INTRODUCTION AND MOTIVATION

By definition, Lyapunov exponents probe the average linear instability of chaotic orbits in an asymptotic $t \to \infty$ limit [1]. Their computation thus involves solving a matrix harmonic-oscillator equation with characteristic frequencies that vary in time. In the context of a geometric description – which is convenient but by no means necessary –, this equation can be reinterpreted as a Jacobi equation (*i.e.,* equation of geodesic deviation) for motion in an appropriately defined curved space, *e.g.,* by introducing the Eisenhart metric [2].

It has been long known [3,4] that geodesic flows in a space with everywhere negative curvature are unstable in the sense that nearby orbits diverge exponentially; and, for this reason, there was an implicit assumption in much earlier work that chaos could often be understood as a manifestation of negative curvature. However, as emphasized by Pettini [5], in many systems chaos cannot be attributed to negative curvature. In many cases, the average curvature is positive; and indeed, there are many known examples of nonintegrable Hamiltonian systems (*e.g.,* the finite order truncations of the Toda [6] potential) which admit large measures of chaos even though the curvature is everywhere positive. The curvature associated with the Eisenhart metric can be negative only if the second derivative of the potential becomes negative. Instead, it would seem natural to understand chaos as reflecting a parametric instability.

The Jacobi equation for a regular periodic orbit reduces to a multi-dimensional Hill equation, *i.e.,* a harmonic-oscillator equation with frequencies that exhibit a periodic time dependence. For certain amplitudes and periodicities, the solutions to such an equation remain bounded (or grow at most as a power law in time), this corresponding to stable periodic orbits. However, for other amplitudes and periodicities, the solutions grow exponentially, this corresponding instead to an unstable periodic orbit [7].

Since chaotic orbits are aperiodic and (in some sense) 'random,' one might instead suppose that one can model the Jacobi equation describing a linearised perturbation of a chaotic orbit as a *stochastic* harmonic-oscillator equation, in which the time-dependent frequencies vary in a random fashion. Given this assumption, the key issue becomes one of identifying the stochastic process, *i.e.* the form of the colored noise, which can capture correctly solutions to the Jacobi equation.

If, for fixed potential and energy, almost all of the constant energy hypersurface is chaotic, as is true generically for $D > 2$ (provided that the energy E is the only time-independent constant of the motion), it would seem reasonable to infer that the parameters for the oscillator equation should be estimatable assuming ergodicity. What this means is that one can assume an invariant measure corresponding to a uniform population of the constant energy hypersurface, *i.e.*, a microcanonical distribution. If, furthermore, one is concerned with comparatively high-dimensional systems, the computationally awkward description in terms of a microcanonical distribution can be replaced by a more user-friendly description based on a canonical distribution: In the spirit of ordinary thermodynamics, one can argue that the canonical and microcanonical ensembles should yield nearly identical results in the large D limit.

Given this logic, Casetti, Clementi, and Pettini [8] developed a 'thermodynamic' theory of chaos which they used to obtain very good estimates of the values of the largest Lyapunov exponents for two well studied physical systems. To do this, they: i) extracted from the

full D-dimensional Jacobi equation an 'isotropized' one-dimensional oscillator equation which they argued should capture the chaotic behavior of typical orbits; (ii) derived the statistics of their assumed stochastic process in the context of a canonical ensemble description; and then (iii) showed that, for two seemingly generic models, solutions to the resulting equation yield reasonable estimates of the largest Lyapunov exponent, at least for $D > 100$ or so.

An obvious question is whether this logic can also be exploited to provide reasonable estimates of the largest Lyapunov exponent for lower dimensional systems, say $D = 2$ or $D = 3$. As discussed in the concluding Section, there are a variety of settings where it would be convenient if one could estimate these values without resorting to detailed numerical computations. Arguably, however, this is *not* the most important point. Rather, the foremost objective is to implement a simple physical picture of the origins of chaos in lower-dimensional Hamiltonian systems. To the extent that the Casetti *et al* proposal, or some variant thereof, can provide reasonable estimates of Lyapunov exponents in these systems, one would seem justified in visualising chaos as arising from a parametric instability manifested by a stochastic-oscillator equation. In other words, one will have a clear new paradigm in terms of which to interpret the origins of chaos in lower-dimensional Hamiltonian systems.

II. AN ILLUSTRATIVE EXAMPLE

The validity of the formula for the largest Lyapunov exponent derived by Casetti *et al.* was tested for one simple toy model. The model is motivated by recent observations of elliptical galaxies, which suggest that these objects can exhibit significant deviations from axisymmetry and that they often have a high-density cusp at their centroids, perhaps associated with the presence of a supermassive black hole. The stars in a real galaxy populate a $6N$-dimensional phase space, with N denoting the number of stars in a system. Considering that fine structure due to localised irregularities and granularity will take a long time to manifest itself, it is of interest to model the system in terms of its coarse-grained 6-dimensional phase space in expectation that the time scale associated with the coarse-grained potential will represent the shortest time scale for macroscopic evolution. Thus, a model potential for such systems comprises the sum of an anisotropic harmonic potential and a spherical Plummer potential:

$$V(x,y,z) = \frac{1}{2}(a^2x^2 + b^2y^2 + c^2z^2) - \frac{M_{BH}}{\sqrt{r^2+\epsilon^2}}, \quad (2.1)$$

with $r^2 = x^2+y^2+z^2$, $a^2 = 1-\Delta$, $b^2 = 1$, and $c^2 = 1+\Delta$. Δ parameterizes the ellipsoidal geometry, and ϵ functions as a "softening parameter" which is set at $\epsilon = 10^{-2}$ for numerical simulations.

The theory of Casetti *et al.*, described in Section IV A below is analytic, and within this formalism ϵ acts as a "free parameter" that reflects uncertainty about the detailed dynamical properties of the phase space. One knows *a priori* that far from M_{BH} the potential it is approximately quadratic in the coordinates, and close to M_{BH} it is approximately spherically symmetric; the orbits are accordingly quasiregular in these regions wherein there will be almost no chaotic mixing. The theory correctly predicts zero chaotic mixing in a harmonic-oscillator potential, thereby incorporating the former circumstance, but it also incorrectly predicts nonzero chaotic mixing in the spherically symmetric Plummer potential that dominates near M_{BH}. Thus, a nonzero ϵ "regularizes" orbits near the black hole. In view of these considerations, the value of ϵ used in the theory was chosen by requiring the magnitude of the harmonic potential to be comparable to a tenth of that of the Plummer potential at distances "$r = \epsilon$" from the centroid. The specific choice is $\epsilon = 0.5M_{BH}^{1/3}$.

FIGURE 1 compares the "true" Lyapunov exponents, computed via numerical simulations with estimates of the largest Lyapunov exponent derived using the Cassetti *et al.* formalism, Eqs. (4.12), (4.15), and (4.16) below. The numerical studies are described in detail in Ref. [9], and the numerically generated curves derive from FIG. 5 in that paper. The figure shows how the Lyapunov exponents pertaining to chaotic orbits scale against black-hole mass and total particle energy E. Interestingly, the analytic results agree closely with the numerical results, particularly for intermediate-to-small values of M_{BH}. The agreement is still reasonable for large values of M_{BH} (values that are in fact unphysically large), though the degree of agreement is less good. This is as expected in that a black-hole mass that is comparable to the ellipsoidal mass will establish sizeable regions of regularity over the constant-energy hypersurface, and the fraction of chaotic orbits will be correspondingly lower [9].

FIGURE 2 compares, for fixed $M_{BH} = 0.1$, the numerical and analytic Lyapunov exponents versus ellipticity as parameterized by Δ. Again, the analytic technique is seen to yield reasonable estimates provided Δ is not too small. As Δ decreases to zero, the potential approaches spherical symmetry and is thereby integrable, supporting only regular orbits. Inasmuch as the fundamental assumption underlying the Casetti *et al.* formalism is that a substantial fraction of the orbits is globally chaotic, the formalism clearly breaks down for spherical symmetry. As discussed in Ref. [9], the fact that the numerical curves exhibit a great deal of structure not manifested by the analytic predictions reflects the fact that the phase space associated with the potential (2.1) is dominated by resonances with frequencies a, b, and c associated with the harmonic contribution which are completely independent of initial conditions.

The results of FIGS. 1 and 2 suggest that the 6-dimensional phase space governed by the toy poten-

tial (2.1) exhibits global chaos and associated rapid irreversible mixing over the bulk of the parameter space. Can the same be said for a lower-dimensional analog, *i.e.* one corresponding to the toy potential in which $z = p_z = 0$? FIGURE 3, which provides the same information as FIG. 1, but now for a 4-dimensional phase space, hints at the answer. One now sees the agreement between the numerical and analytic results to be less good, as would be expected because the fraction of globally chaotic orbits is generally much reduced over the 6-dimensional case. Nonetheless, the results are still comparable within a factor of two.

III. THE SCOPE OF THIS PAPER

The obvious question is whether the striking agreement between theory and numerics described in the preceding section is simply a fortuitous accident, or whether it is in fact generic. Can the Casetti *et al.* analysis provide reasonable estimates of the largest Lyapunov exponent for generic lower-dimensional Hamiltonian systems?

Related to this is another important question: To what extent are the assumptions implemented by Casetti *et al* justified for lower-dimensional systems? To the extent that they are *not* justified, one might expect either (i) that the final formula for χ which they derived is comparatively insensitive to (some of) the assumptions and/or (ii) that modifying these assumptions might lead to improved estimates.

These questions were addressed by a detailed exploration of orbits in the potentials discussed in Section II, as well as three other (classes of) potentials:

1. The sixth order truncation of the Toda lattice [6], a familiar two-dimensional potential:

$$V(x,y) = \frac{1}{2}\left(x^2+y^2\right) + x^2y - \frac{1}{3}y^3 + \frac{1}{2}x^4 + x^2y^2 + \frac{1}{2}y^4 + x^4y + \frac{2}{3}x^2y^3 - \frac{1}{3}y^5 + \frac{1}{5}x^6 + x^4y^2 + \frac{1}{3}x^2y^4 + \frac{11}{45}y^6. \tag{3.1}$$

2. A multi-dimensional generalisation of the dihedral potential [10], for one particular set of parameter values, allowing for $D = 2$ through $D = 6$:

$$V(q_1,..,q_D) = -\sum_{i=1}^{D} q_i^2 + \frac{1}{4}\left(\sum_{i=1}^{D} q_i^2\right)^2 - \frac{1}{4}\sum_{i<j=1}^{D} q_i^2 q_j^2. \tag{3.2}$$

3. A generalisation of the Fermi-Pasta-Ulam (*FPU*) β model [11] with

$$V(q_1,..,q_D) = \sum_{i=1}^{D}\left[\frac{a}{2}\left(q_{i+1}-q_i\right)^2 + \frac{b}{4}\left(q_{i+1}-q_i\right)^4\right], \tag{3.3}$$

with $q_{D+1} \equiv q_1$, allowing for $D = 3$ through $D = 6$ (the special case $D = 2$ is integrable). For $a = 1$, (3.3) reduces to the standard *FPU* model; for $a < 0$, the potential admits extrema that are local maxima, so that the local mean curvature can become negative. The case $a = 1$ and $b = 0.1$ was considered by Casetti *et al.* for much larger values of D.

Section IV of this paper begins by providing a terse mathematical summary of the formalism introduced by Casetti *et al.* to estimate the values of the largest Lyapunov exponent in higher-dimensional systems. This mathematical structure is then restated in much simpler physical language and the resulting reformulation is used to suggest how their analysis could be reformulated for lower-dimensional systems. Section V summarises the results of extensive simulations in the potentials (2.1) and (3.1) - (3.3) which were used to test the validity of the original assumptions. Section VI then turns to the actual values of Lyapunov exponents estimated using this general approach, considering both the 'true' Lyapunov exponents, defined in a $t \to \infty$ limit, and short-time Lyapunov exponents [12] appropriate for orbit segments of comparatively short duration. Estimates of the latter for a variety of different orbit segments evolved in the same potential with the same energy reveals an important point: Even when the estimated short-time exponents χ_{est} differs from the 'true' exponents χ_{num} computed numerically by as much as a factor of two, their values tend to be strongly correlated. For example, orbit segments for which χ_{est} is especially small correspond in general to orbits for which the numerical χ_{num} is also especially small. In this sense, it is clear that, even if the Casetti *et al.* formula for χ is not completely satisfactory, it *does* capture some important aspects of the flow. Section VII concludes by summarising the principal conclusions and discussing potential implications and extensions.

IV. CHAOTIC MOTION AS A STOCHASTIC PARAMETRIC INSTABILITY

A. The proposal of Casetti, Clementi, and Pettini

The starting point is the reformulation of a time-independent Hamiltonian system as a geodesic flow in an appropriately defined curved space. This can be done in a variety of different ways, the best known of which involves implementing Maupertuis' Principle [13], which leads to the Jacobi metric. However, from a practical perspective, the most convenient choice is to work with the Eisenhart metric [2].

Given a D degree-of-freedom Hamiltonian system characterised by a Lagrangian

$$L = T - V = \frac{1}{2}a_{ij}\dot{q}^i\dot{q}^j - V(q^1,...,q^D), \tag{4.1}$$

with motion defined on some manifold M, consider the extended manifold $M \times R^2$, with coordinates $(q^0, q^1, ..., q^D, q^{D+1})$, and introduce the Eisenhart metric

$$\begin{aligned} ds^2 &= g_{\mu\nu} dx^\mu dx^\nu \\ &= a_{ij} dq^i dq^j - 2V(q) dq^0 dq^0 + 2 dq^0 dq^{D+1}. \end{aligned} \tag{4.2}$$

Setting $q^0 = t$ and $q^{D+1} = t/2 - \int_0^t dt' L(\mathbf{q}, \dot{\mathbf{q}})$ yields $ds^2 = dt^2$. Without loss of generality one can set $a_{ij} = \delta_{ij}$, making the kinetic energy a sum of quadratic contributions $(\dot{q}^i)^2/2$, in which case the geodesic equations reduce to Newton's equations of motion. Correspondingly the Riemann tensor simplifies greatly; its only nonvanishing components are

$$R_{0i0j} = \frac{\partial^2 V}{\partial q^i \partial q^j}, \tag{4.3}$$

and the Jacobi equation for a linearised perturbation becomes

$$\ddot{\xi}^i + \delta^{ij} R_{0j0k} \xi^k = 0, \qquad (i = 1, ..., D). \tag{4.4}$$

Were the Riemann components entering into Eq. (4.4) were everywhere negative, an arbitrary perturbation would always grow exponentially fast. Everywhere negative curvature implies chaotic behavior and positive Lyapunov exponents [3,4]. The important point, however, is that, because of parametric instability, one can have chaotic orbits with positive Lyapunov exponents even if the curvature is everywhere positive. If, following Casetti *et al.*, one assumes that the curvature varies 'randomly' along a chaotic orbit, eq. (4.5) reduces to a stochastic-oscillator equation of the form

$$\frac{d^2 \xi^i}{dt^2} + k^i{}_j(t) \xi^j = 0, \qquad (i = 1, ..., D), \tag{4.5}$$

where the matrix $k^i{}_j$ is characterised completely by its statistical properties. However, it is well known that, even if $k^i{}_j$ is positive definite for all times, ξ^i can grow exponentially [14].

Especially in high dimensions, matrix equations become difficult to solve either numerically or analytically. For this reason, Casetti *et al.* proceeded by replacing this D-dimensional equation with a simpler one-dimensional equation which aims to capture its 'average' behavior. Formally, they start by observing that the Riemann tensor can be decomposed into two pieces:

$$R^i{}_{jkl} = \frac{1}{D-1} \left(R_{jl} \delta^i_k - R_{jk} \delta^i_l \right) + W^i{}_{jkl} \tag{4.6}$$

where R_{ij} the Ricci tensor and $W^i{}_{jkl}$ is the Weyl projective tensor. For the case of an isotropic space, the Weyl tensor vanishes identically and $R_{jl} \dot{q}^j \dot{q}^l / (D-1)$ reduces to the (constant) sectional curvature. The crucial assumption then is that, even though the space is not isotropic, it should appear nearly isotropic when viewed on comparatively large scales. In the context of such a 'quasi-isotropic' approximation, $R^i{}_k$ and $w^i{}_k = \delta^{ij} W^l{}_{jlk}$ become diagonal, and Eq (4.6) reduces to a one-dimensional equation of the form

$$\frac{d^2 \xi}{dt^2} + k(t) \xi = 0. \tag{4.7}$$

All that remains is to specify the statistical properties of the random process $k(t)$.

For a generic Hamiltonian system, the form of k could be quite complex. However, given the assumption that D is large, one might expect that the complicated details will largely wash out. Thus, Casetti *et al.* argue in the spirit of the Central Limits Theorem that the curvature fluctuations in different directions can be approximated as nearly independent and, at any instant, Gaussianly distributed. It then follows that

$$\frac{d^2 \xi}{dt^2} + \Omega \xi + \sigma \eta \xi = 0, \tag{4.8}$$

where, in terms of the quantity $K = \partial^2 V / \partial q^i \partial q_i \equiv \Delta V$, which has mean $\langle K \rangle$ and dispersion δK, the quantity $\Omega = \langle K \rangle / (D-1)$, $\sigma = \delta K / \sqrt{D-1}$, and η is Gaussian noise with zero mean and unit variance. The factors involving D reflect the fact that the curvature-driven motion in the i^{th} direction is, on the average, 'shared' by the $D-1$ orthogonal directions.

Presuming further that the flow is ergodic and that (almost) all orbits are chaotic, the quantities $\langle K \rangle$ and δK can be calculated assuming a uniform sampling of the constant energy hypersurface, *i.e.,* a microcanonical distribution $\mu \propto \delta_D(H - E)$. Alternatively, for sufficiently high dimensions one can proceed instead by assuming a canonical distribution which, for large D, is much simpler computationally although it should yield nearly identical results.

To complete the characterisation of the random process $k(t)$ it remains to specify the autocorrelation function $\Gamma(t)$ or, at least, the autocorrelation time τ, which governs how rapidly the curvature fluctuates along the orbit. This Casetti *et al.* provide using another geometric argument. On the one hand, they identify a time scale

$$\tau_1 \approx \frac{\pi}{2\sqrt{\Omega + \sigma}} \tag{4.9}$$

corresponding to the typical time between successive conjugate points, *i.e.,* points where the Jacobi field of geodesic deviation vanish. On the other, they identify a time scale

$$\tau_2 \approx \frac{\Omega^{1/2}}{\sigma} \tag{4.10}$$

corresponding to the length scale on which the fluctuations become comparable to the average curvature. They

then select as an appropriate autocorrelation time a value τ satisfying

$$\tau^{-1} = 2\left(\tau_1^{-1} + \tau_2^{-1}\right) \tag{4.11}$$

so that

$$2\tau = \frac{\pi\sqrt{\Omega}}{2\sqrt{\Omega\left(\Omega+\sigma\right)} + \pi\sigma} \tag{4.12}$$

Casetti *et al.* suggest further that $\Gamma(t)$ might be well approximated by the oscillating function

$$\Gamma(t) = \frac{\Omega^2}{\pi}\,\frac{\sin\omega t}{\omega t}, \tag{4.13}$$

which yields an autocorrelation time

$$\tau = \frac{1}{2\omega} = \frac{\tau_{osc}}{4\pi}, \tag{4.14}$$

with τ_{osc} the oscillation period. However, this is largely irrelevant for their analysis. Granted the assumption of additive Gaussian noise, the form of the color only enters into the final expression for χ through the autocorrelation time τ [14].

Given a knowledge of τ and the first two moments, Eq. (4.8) can be solved analytically using a technique developed by van Kampen [14] to yield an estimated largest Lyapunov exponent

$$\chi = \frac{1}{2}\left(\Lambda - \frac{4\Omega}{3\Lambda}\right), \tag{4.15}$$

where

$$\Lambda = \left[2\sigma^2\tau + \sqrt{\left(\frac{4\Omega}{3}\right)^3 + \left(2\sigma^2\tau\right)^2}\,\right]^{1/3}. \tag{4.16}$$

B. Applying this proposal to lower-dimensional Hamiltonian systems

The preceding can be reformulated without recourse to differential geometry in a setting that makes the physical content of the assumptions more transparent and, as such, makes it clearer which assumptions might prove suspect, especially for lower-dimensional systems.

The basic perturbation equation (4.5) can be derived trivially from the original Hamilton equations

$$\frac{dq^i}{dt} = \frac{\partial H}{\partial p_i} = \delta^{ij}p_j \tag{4.17}$$

and

$$\frac{dp_i}{dt} = -\frac{\partial H}{\partial q^i} = -\frac{\partial V}{\partial q^i} \tag{4.18}$$

associated with the Hamiltonian

$$H = T + V = \frac{1}{2}\delta^{ij}p_ip_j + V(q). \tag{4.19}$$

It is clear that the introduction of a small perturbation $q^i \to q^i + \xi^i$ and $p_i \to p_i + \zeta_i$ leads to evolution equations of the form

$$\frac{d\xi^i}{dt} = \delta^{ij}\zeta_j \qquad \text{and} \qquad \frac{d\zeta_i}{dt} = -\frac{\partial^2 V}{\partial q^i \partial q^j}\xi^j, \tag{4.20}$$

but combining these last two equations leads immediately to Eq. (4.4).

The crucial assumption underlying the entire Casetti *et al.* analysis is the assumption that, for the case of chaotic orbits, Eq. (4.4) can be modelled by a stochastic-oscillator equation. For the case of 'wildly chaotic' orbits or orbit segments, which are far from periodic, this assumption would seem quite reasonable. However, in lower dimensional systems one encounters the possibility of 'sticky' [15] orbit segments which, albeit characterised by positive short-time Lyapunov exponents, are 'nearly regular' in visual appearance and have Fourier spectra with most of the power concentrated at or near a few special frequencies [16]. This is especially common for $D = 2$, where cantori [1] can serve as entropy barriers, confining a chaotic orbit near a regular island for surprisingly long times. To the extent that such orbit segments behave in a nearly regular fashion, the assumption of nearly random behavior is clearly suspect, and one might anticipate that a stochastic oscillator equation cannot prove completely satisfactory. Alternatively, to the extent that this 'sticky' behavior is rare, such an equation might be expected to provide a reasonable starting point.

The assumption of 'quasi-isotropy' can also be understood in very simple physical terms: Instead of considering the D-dimensional Eq. (4.4), which involves the full second derivative matrix of V, it is assumed that, on the average, each direction in configuration space is statistically identical, so that one can consider instead D identical one-dimensional equations. In this context, the only question concerns the proper identification of the quantity to play the role of the squared frequency $k(t)$. The Casetti *et al.* prescription atates that the relevant information about stability is contained in the trace of the second derivative matrix, so that $k(t)$ should be proportional to $\Delta V = \partial^2 V/\partial q^i \partial q_i$. The factor of $D-1$ entering into Eq. (4.8) reflect the fact that the perturbation driving the chaos is 'shared' amongst $D-1$ dimensions. (Recall that, in a time-independent Hamiltonian system, there is always one direction of neutral stability corresponding to translation along the orbit from $q^i(t)$ to $q^i(t+\delta t)$.)

This assumption of quasi-isotropy seems especially reasonable for large D where, on average, different directions of the configuration space should look much the same, but becomes more suspect in lower dimensions. In principle, one can relax this assumption by working with the

full matrix equation. As a practical matter, however, this becomes quite cumbersome for $D \gg 2$. For this reason, most the following analysis will retain the assumption of quasi-isotropy. What happens when this assumption is relaxed for two-dimensional systems is considered briefly in Section VI. It would in fact appear that, at least for $D = 2$, relaxing this assumption does not in general yield significant improvement in the estimated value of the largest Lyapunov exponent.

For generic Hamiltonian systems with large D one anticipates that (almost) all the orbits on a constant-energy hypersurface are chaotic. Granted the assumption of ergodicity, it then follows that, over sufficiently long time scales, an orbit eventually samples a microcanonical distribution. This implies that, when estimating a Lyapunov exponent $\chi(E)$, as defined in an asymptotic $t \to \infty$ limit, one can assume that the statistical properties of the curvature experienced by an orbit are given correctly by a microcanonical distribution. By contrast, for lower dimensional systems, especially $D = 2$, one anticipates instead that a generic potential will admit a coexistence of large measures of both regular and chaotic orbits, so that the assumption of a microcanonical distribution is *not* justified. Rather, granted the assumption of ergodicity, one would anticipate the existence of a different invariant distribution, corresponding to a uniform population of those portions of the constant energy hypersurface which are accessible to a chaotic orbit with specified initial condition. It is not clear how this distribution could be computed analytically. However, as described in Section V, numerical approximations to this invariant distribution can be generated straightforwardly through a time-series analysis of orbits evolved numerically.

Even if a microcanical distribution is justified, the assumption of Gaussian fluctuations is problematic. For large D, this assumption can be motivated with a fair degree of rigor via a Central Limits Theorem argument, supposing that the distribution of values of ΔV involves a convolution of D nearly independent distributions for the separate components $\partial^2 V/\partial q^i \partial q^i$ (no sum over indices). For very small D, this is clearly not justified, and the minimum value of D for which the Gaussian approximation *is* justified must depend to a certain extent on the form of the individual distributions. It will be seen in Section V that, for the model systems (3.2) and (3.3), the convergence towards a Gaussian is quite efficient, and that the distribution $N[\Delta V]$ is reasonably well fit by a Gaussian even for D as small as 3 or 4. It will also be seen that, at least for distributions $N[\Delta V]$ that are not too skew, deviations from a Gaussian do not change the estimated value of the largest Lyapunov exponent all that much.

The formula for the autocorrelation time τ motivated by Casetti *et al.* is somewhat *ad hoc* in that, unlike the other crucial inputs Ω and σ, it cannot be derived directly from a microcanonical distribution. However, the basic scaling implicit in τ can again be inferred relatively simply. As will be seen below, Ω and σ are typically comparable in magnitude. They both reflect statistical properties of ΔV and, as such scale (within factors of order unity) as $\overline{V}/R^2$, where $\overline{V}$ represents a typical value of potential and R is a characteristic length scale, *i.e.,* the size of the configuration space region probed by an orbit. Assuming 'virialisation,' *i.e.*, that the mean potential and kinetic energies of the orbits are comparable in magnitude, it follows that $\overline{V} \sim v^2$, where v denotes a typical orbital speed. However, this implies that $\Omega \sim \sigma \sim v/R \equiv t_D^{-1}$, where t_D denotes a characteristic dynamical or crossing, time. Allowing for the fact that the characteristic scale on which V changes significantly is typically somewhat smaller than the size of region accessible to the orbit leads to the obvious physical conclusion that τ should be comparable to, but somewhat smaller than, the time required for an orbit to travel from one side of the system to another.

Implicit in the Casetti *et al.* analysis is the assumption that the stochastic process $k(t)$ corresponds to state-independent, additive noise, so that, *e.g.,* the autocorrelation time τ on which the curvature changes is independent of the value of the curvature. Strictly speaking, this assumption cannot be correct. If, *e.g.,* an orbit is in a region where V is especially small, its kinetic energy, and hence its velocity, will be especially large, so that the orbit will move very quickly to a different region where V, and hence in general ΔV, is very different. If, instead, the orbit is in a region where V is especially large, it will move more slowly so that ΔV might be expected to change more slowly. The autocorrelation time τ of (4.13) represents an average over a variety of orbits with very different values of V. One might anticipate that these differences will tend to wash out for large D, but there is no obvious reason why this should be true for smaller D.

One final point: It is clear that, for small D, one cannot pass from a microcanonical to a canonical description. One must work directly with the microcanonical measure $\mu \propto \delta_D(H - E)$. This, however, is not a major problem. For a D degree of freedom system, the microcanonical distribution corresponds to a configuration space density

$$f(q^i) \propto \begin{cases} (E-V)^{(D-2)/2} & \text{if } V \leq E; \\ 0 & \text{if } V > E. \end{cases} \tag{4.21}$$

but, given this formula for f, it is straightforward, at least numerically, to compute the distribution $N[\Delta V]$ and/or any moments of the distribution.

V. TESTING THE BASIC ASSUMPTIONS

A. What was computed

To test the validity of the basic assumptions requires a comparison of real orbital data with predictions made assuming a microcanonical distribution. The requisite orbital data were generated and analyzed as follows:

For given choices of potential and total energy, a collection of $N = 1000$ initial conditions were selected, and each of these was integrated into the future for a total time T corresponding to between ~ 100 and 2000 characteristic crossing times t_D. The numerical integration simultaneously tracked the evolution of a small initial perturbation, periodically renormalised in the usual way [1] so as to yield an estimate of the largest (short-time) Lyapunov exponent for the orbit segment. Configuration space data, recorded at fixed intervals δt, were used to generate a time series $\{K_j(n\delta t)\}$ for each of the segments in the 1000 orbit ensemble which was deemed to be chaotic. δt was typically so chosen that each segment was sampled by 2560 points. Distinctions between regular and chaotic were implemented through the introduction of a threshhold value χ_{min}: if the computed $\chi < \chi_{min}$, the orbit segments were assumed to be regular. Combining all the orbital data for all the chaotic orbits allowed the computation of the bulk moments $\langle K\rangle$ and δK where, recall, $K = \Delta V$. Binning the combined data into 1000 bins yielded a numerical representation of the distribution $N[K]$.

A discretized representation of the average autocorrelation function $\Gamma(t)$ was computed by selecting a representative ensemble of 5120 initial conditions, evolving each of these into the future for an extended time $T \geq 2048$, so as to generate a set of well-mixed 'random' phase space points, identifying each of the $N_c \leq N$ orbit segments that were chaotic, and, by extending the integrations for an additional time $T' = 1024$, constructing

$$\Gamma(n\delta t) = \frac{1}{N_c\langle K^2\rangle}\sum_{j=1}^{N_c} DK_j(T)DK_j(T+n\delta t). \quad (5.1)$$

Here $DK_j \equiv K_j - \langle K\rangle$, and the quantities $\langle K\rangle$ and $\langle K^2\rangle$ represent averages computed for all the chaotic orbital data for $T < t < T'$. Ideally one should compute the autocorrelation time τ using the defining relation

$$\int_0^\infty dt\,\Gamma(t) = \langle K^2\rangle\tau. \quad (5.2)$$

Given, however, that Γ is typically a rapidly oscillating function (period $\sim t_D$) with an envelope that damps very slowly, such a computation proved unreliable. A seemingly better measure of τ or, at least, of how τ scaled with energy E for fixed potential, was obtained by computing the period τ_{osc} associated with the oscillations.

Predictions associated with a microcanonical distribution were computed as follows: The microcanonical distribution $\mu \propto \delta_D(H-E)$ implies the configuration space probability density (4.22); but, given this f, it is straightforward to compute the value of any configuration space function $g(q)$. Numerical representations of the distribution $N[K]$ associated with a microcanonical distribution were computed by dividing the occupied configuration space into a collection of M hypercubes, (ii) deciding randomly whether or not to sample each hypercube, using a weighting $\propto (E-V)^{(D-2)/2}$ as evaluated at a random point in the cube, (iii) in the event that the hypercube was to be sampled, locating a point in the cube at a randomly chosen location, and then (iv) binning the resulting collection of points into 1000 bins.

Granted the assumption of a Gaussian distribution of curvatures, estimates of the Lyapunov exponent χ can be, and were, computed using eq. (4.16), which does not require the assumption of a microcanonical population. When the assumption of a Gaussian distribution is relaxed, an analytic solution is not possible in general, so that χ was obtained instead from a numerical computation, with the random curvature generated initially by sampling $N[K]$, held constant for the autocorrelation time τ, and then replaced by another, randomly chosen curvature [17].

B. What was found

1. $N[K]$ and its first two moments

FIGURE 4 exhibits the energy-dependence of the quantities $\langle K\rangle$ and δK for chaotic orbits in the dihedral potential with $D = 2$ and $D = 3$, computed both from time-series data (dashed lines) and assuming a microcanonical distribution (solid lines). Overall, one observes excellent agreement between the numerical and analytic predictions, particularly for the first moment $\langle K\rangle$. The best overall agreement obtains for lower energies where, even for $D = 2$, the measure of regular orbits is comparatively small and 'stickiness' seems comparatively unimportant.

For $D = 2$ at higher energies, say $E > 1.0$ or so, it appears that a third of the constant energy hypersurface, or even more, corresponds to regular orbits, so that one is clearly *not* justified in assuming a microcanonical distribution. However, it is evident that the predictions based on a microcanonical distribution remain quite good. That this should be the case is not really surprising. Presuming that the regular islands are not concentrated preferentially at regions where ΔV is especially large or small, it would seem reasonable to assume that, in a sufficiently coarse-grained sense, chaotic orbits still go 'all over' the energetically allowed regions of configuration space. To the extent, however, that this be true, one might expect moments approximating the moments appropriate for a microcanonical distribution which, for $D = 2$, implies [cf. Eq. (4.21)] a uniform configuration space density. FIGURE 5 exhibits analogous data for the *FPU* potential with $D = 4$ and $D = 6$, generated for parameter values $a = 1.0$ and $b = 0.1$.

The thick solid curves in panels (a) - (d) of FIG. 6 exhibit distributions of curvatures, $N[K]$, for the dihedral potential with $D = 2$ and $D = 6$ generated assuming a microcanonical distribution. The corresponding curves

in FIG 7 exhibit analogous distributions for the FPU potential for $D = 4$ and $D = 6$. Panels (e) and (f) in FIG. 6 show the time series and microcanonical predictions for the dihedral potential in (from left to right) $D = 3$, 4, and 5. It is evident that the microcanonical distributions for the dihedral potential with $D = 2$ are not even remotely Gaussian in shape. However, it is also apparent that, for all the other cases, the distribution is in fact reasonably well fit by a Gaussian, although $N[K]$ typically has a slight skew and can manifest appreciable deviations for large $|K - \langle K \rangle|$.

The other curves in FIG. 6 (a) - (d) and in FIG. 7 represent distributions $N[K]$ generated from time-series data. FIG. 7 and the first three panels of FIG. 6 display two numerical curves, one representing data for $0 < t < 1024$ and the other for $2048 < t < 3072$. FIG. 6 (d) also includes a third numerical curve, generated for $8192 < t < 9216$. For the two energies exhibited in the $D = 2$ dihedral potential, $E = 1.0$ and $E = 6.0$, there exist large measures of both regular and chaotic orbits and, for this reason, the time-series $N[K]$ differs significantly from the microcanonical $N[K]$. However, the ensembles of initial conditions used to generate the time-series distributions evolved towards an invariant (albeit non-microcanonical) distribution relatively quickly, so that the two numerical curves very nearly overlap.

For the dihedral potential with $D \geq 3$ and for the FPU potential with $D \geq 4$ almost all the orbits appear to be chaotic, so that, assuming ergodicity, the microcanonical $N[K]$ and a truly representative time-series $N[K]$ should coincide up to statistical uncertainties. However, for the cases exhibited in FIGS. 6 (c) and (d) and FIG. 7, the initial ensembles only converged towards an invariant distribution on a comparatively long time scale, so that the two (or more) time-series curves differ appreciably from one another. In each case, the later time sampling(s) yielded distributions $N[K]$ that more closely approximated the microcanonical $N[K]$.

The preceding suggests that one can use the form of the distribution $N[K]$ as a robust diagnostic in terms of which to probe the approach towards ergodicity. Ergodicity *per se* is an assumption regarding the $t \to \infty$ limit and, even assuming ergodicity, there remains an obvious question: How long must one evolve some ensemble of initial conditions before its time-averaged density closely approximates the density associated with a constant population of the accessible phase space regions? Comparing the distribution $N[K]$ associated with an evolving ensemble with the $N[K]$ associated with a microcanonical distribution can provide a useful diagnostic for probing the extent to which the ensemble has evolved towards a time-independent invariant distribution.

It is well known that different chaotic orbit segments in the same connected phase space region can exhibit vastly different short-time Lyapunov exponents, and that the values of these short-time exponents can correlate significantly with position. For example, chaotic segments near regular islands tend to be much less unstable than wildly chaotic segments located in the middle of the stochastic sea. One might, therefore, expect that orbit segments with especially large or small short-time exponents would be characterised by different curvatures. For potentials and energies where almost all the orbits are chaotic and 'stickiness' is rare, this segregation should be minimal; but for potentials where there is a coexistence of large measures of both regular and chaotic orbits, and where 'stickiness' is pronounced, this effect should be much more pronounced.

As illustrated in FIG. 8, this intuition was corroborated numerically. The top panel of FIG. 8 was generated for $E = -0.5$ in the $D = 2$ dihedral potential, an energy where the regular regions are extremely small, so that a representative ensemble of 1000 initial conditions, integrated for a time $T = 1024$, yielded no regular orbits. The orbits generated from these initial conditions were divided into five quintiles, depending on the values of their short-time Lyapunov exponents, and the lower five curves in this panel exhibit individual subdistributions $N[K]$ computed for each quintile. The four quintiles corresponding to the larger values of χ yielded distributions that were nearly identical. The lowest quintile was again quite similar, but did manifest some noticeable differences: This subdistribution, corresponding to the thick solid line, is distinctly underrepresented at very low values of K and over-represented at very large K, and, unlike the other four quintiles, appears to be a slowly decreasing function of K in the interval $0 < K < 7.5$. The sum of these five subdistributions (with a different normalisation from the subdistributions) corresponds to the slightly jagged upper curve, which is essentially identical, modulo statistical uncertainties, to the smoother curve computed for a microcanonical distribution.

The lower panel of FIG 8 exhibits analogous data for $E = 6.0$, again in the $D = 2$ dihedral potential. In this case, a 1000 orbit ensemble was divided instead into a 'quintile' of 332 regular orbits and four 'quintiles' each comprised of 167 chaotic orbits, but the resulting subensembles were analyzed identically. The lower solid curve peaking at $K \sim 13$ represents the 332 regular orbits, and the three nearly identical curves which have a local minimum at $K \sim 13$ correspond to the chaotic orbit segments with the largest short-time Lyapunov exponents. The intermediate dashed curve corresponds to the chaotic orbits with the smallest short-time Lyapunov exponent, the majority of which could be reasonably classified as 'sticky.' The total $N[K]$ given as a sum of the four chaotic 'quintiles' is represented by the upper curve with a local minimum at $K \sim 13$. The upper curve corresponding to a nearly flat profile again corresponds to a microcanonical distribution.

2. The autocorrelation time τ

As suggested by Casetti *et al.*, the autocorrleation function $\Gamma(t)$ is in fact an oscillating function of time, but it tends to decay more slowly than with the $1/t$ envelope implicit in Eq. (4.14). This slower decay is especially evident for potentials and energies when 'stickiness' is important, in which case a substantial 'memory' can persist for dozens of oscillations. This is, *e.g.,* evident in FIG. 9 (a) - (d), which exhibit data for the dihedral potential for $D = 2$ and $D = 6$. The first two panels correspond to a very low energy $E = -0.5$, where, even for $D = 2$, almost all the orbits are chaotic. The second two panels correspond to a higher energy $E = 6.0$ where, for both $D = 2$ and $D = 6$, chaotic segments can be nearly periodic and have comparatively small short-time Lyapunov exponents. For $D = 2$, the case exhibited in panel (c), roughly one quarter of the chaotic orbits are noticeably 'sticky'; for $D = 6$, the case in panel (d), the fraction is reduced to about 5%. In either case, analysis of a sample that excludes 'sticky' segments yields an autocorrelation function that decays substantially more quickly.

As noted by Casetti *et al.*, if the autocorrelation function is in fact well approximated by Eq. (4.13) the time scale identified geometrically in Eq. (4.12) should coincide with the time scale (4.14). This prediction was tested numerically and found typically to be satisfied to within factors of $\sim$2, although some discrepancies were observed. As noted already, a direct determination of τ using Eq. (5.2) proved unreliable.

Perhaps the most striking point is that, at least when 'stickiness' is comparatively unimportant, the Casetti *et al.* time scale τ given by Eq. (4.13) and the time scale τ_{osc} exhibit very similar scaling with energy E. This is illustrated in FIG. 9 (e) and (f), which exhibit both time scales as functions of E for the $D = 2$ and $D = 6$ dihedral potential. In each case, the time scale τ_{osc} is somewhat longer than the Casetti *et al.* time scale τ. Significantly, though, for $D = 2$ the quantities τ_{osc} and τ exhibit very different scalings at higher energies, precisely where 'stickiness' is most prominent.

3. Sources of uncertainty

Granted the assumption of a Gaussian distribution of curvatures, the predicted value of the largest Lyapunov exponent depends on only three quantities, namely $\langle K \rangle$, δK, and τ; and as such, it is natural to ask how the predicted value χ_{est} varies if any of these inputs are changed.

If one introduces a simulataneous scaling of both $\langle K \rangle$ and δK, *i.e.,* $\langle K \rangle \to \alpha \langle K \rangle$ *and* $\delta K \to \alpha \delta K$, with α of order unity, $\chi_{est} \to \alpha^{1/2} \chi_{est}$. If, alternatively,$\langle K \rangle$ is held fixed but $\delta K \to \alpha \delta K$, one infers, at least approximately, that $\chi_{est} \to \alpha^{3/2} \chi_{est}$. Finally, if $\langle K \rangle$ and δK are held fixed, but one allows for a scaling $\tau \to \alpha \tau$, $\chi_{est} \to \alpha \chi_{est}$.

Given that the values of $\langle K \rangle$ and δK can be estimated quite well using simple dimensional arguments – recall that, even when there are relatively large measures of periodic orbits, a microcanonical population yields estimates in good agreement with the results of direct numerical computation –, it would seem that, with the assumption of quasi-isotropy and a Gaussian distribution of curvatures, the largest source of error should be in the determination of the autocorrelation time τ. The expression for τ motivated by Casetti *et al.* is more *ad hoc* than the expression for $\langle K \rangle$ and δK; and dimensional arguments are hard pressed to yield estimates of τ that are accurate to better than a factor of two. However, factors of two uncertainty in τ translate directly into factors of two uncertainty in χ_{est}.

One can also investigate how the predicted χ_{est} changes if one relaxes the assumption of a Gaussian distribution, instead computing χ_{est} by solving Eq. (4.9) numerically for the distribution $N[K]$ generated either from a microcanonical distribution or from real orbital data. The resulting change in χ_{est} will of course depend on the degree to which $N[K]$ deviates from a Gaussian, larger deviations resulting in larger changes. Especially for two-dimensional systems, whre $N[K]$ is far from Gaussian, allowing for the correct distribution can change χ_{est} by factor of three, or even more.

This is illustrated in FIG. 9, which exhibits several different estimates of the largest Lyapunov exponents χ_{est} for the $D = 2$ dihedral potential, most of which will be described in Section VI. In the present context, note simply (i) the 'true' χ_{num}, generated by tracking a small initial perturbation (solid line), (ii) the Casetti *et al.* χ_{est}, based on the assumption of Gaussian fluctuations and an autocorrelation time given by Eq. (4.13) (short dashes), and (iii) an alternative χ_{est}, again based on the 'quasi-isotropized' Eq. (4.9), but now allowing for a distribution $N[K]$ generated from time-series data and an autocorrelation time (4.15) (long dashes). Both estimates are comparable in magnitude to χ_{num}, but both miss the nontrivial dip that arises near $E = 0.0$.

VI. ESTIMATES OF LYAPUNOV EXPONENTS IN LOWER-DIMENSIONAL HAMILTONIAN SYSTEMS

A. Estimates of the true Lyapunov exponent

Overall, Eq. (4.15) first proposed by Casetti *et al.*, modified to allow for moments computed assuming a microcanonical distribution, appears to give reasonable estimates of the largest Lyapunov exponent in lower-dimensional Hamiltonian systems, provided that an appreciable fraction of the phase space corresponds to chaotic orbits. In particular, as long as the true Lyapunov exponents are not very small ($\chi_{num} \not\ll t_D^{-1}$) and/or 'stickiness' is not especially prominent, the estimated χ_{est}

typically agree with the numerical χ_{num} to within factors of two. In some cases, such as for the *FPU* model, the agreement between χ_{num} and χ_{est} rapidly increases with increasing D; but in other cases, such as for the dihedral potential, this is *not* the case. This would suggest that the quasi-isotropy assumption, which should become increasingly justified in higher dimensions, is *not* necessarily the principal source of error.

FIGURE 11 compares the numerical and estimated $\chi(E)$ for the dihedral potential for $D = 2$, 3, 4, and 6. The estimated values were computed using Eq. (4.13), based on a Gaussian distribution, with moments generated both from a time-series analysis (dashed lines) and assuming a microcanonical distribution (dotted lines). The numerical values are connected with a solid line. One observes significant differences in the shapes of the curves associated with the numerical and estimated values, but there is invariably an overall agreement to within a factor of two. The most striking discrepancies arise for $D = 2$, where the estimates completely miss the abrupt dip in χ_{num} for $E \sim 0$. The fact that, for $D = 2$, the two estimated curves differ significantly at high energies reflects the fact that the constant energy hypersurface contains large regular islands, so that the invariant distribution is far from microcanonical.

FIGURE 12 exhibits the numerical and estimated $\chi(E)$ for the *FPU* model for $D = 4$, 5, and 6, with the estimated values again computed assuming Gaussian distributions and moments generated from a time-series analysis. The data have been plotted on a log-log plot to facilitate comparison with FIG. 3 in Casetti *et al.* Here two points are immediately obvious: (1) The estimated and numerical curves are distinctly different, with χ_{est} always larger than χ_{num}, but their curvatures are comparatively similar. (2) The agreement between χ_{num} and χ_{est} becomes progressively better for higher dimensions and for higher energies. For $E = 5$ in $D = 4$, where the numerical $\chi_{num} = 0.211$ corresponds to a very long time $t \sim 45 \gg t_D$, χ_{est} overestimates χ_{num} by nearly a factor of seven. For $D = 6$ and $E = 5$, χ_{est} yields a value approximately 2.65 times too large; for $E = 10240$, its value is only 1.27 times too large.

FIGURE 13 (a) exhibits the same data for the sixth order truncation of the Toda potential. As for the *FPU* model, χ_{est} systematically overestimates the true χ_{num}, the largest errors arising at low energies, where χ_{num} is comparatively small, larger regular islands exist, and 'stickiness' is especially important.

B. Short-time Lyapunov exponents

The computations described in the preceding subsection indicate that, for a variety of lower-dimensional systems, the Casetti *et al.* model of a stochastic-oscillator equation yields reasonable estimates of the largest Lyapunov exponent, χ, as a function of energy E. However, if the stochastic-oscillator picture is to be accepted as completely valid, one must also demand that it 'explain' the varying degrees of chaos manifested by different chaotic orbit segments with the same energy, as probed by short time Lyapunov exponents. In particular, one might hope that, even if the estimated values χ_{est} of the true Lyapunov exponent disagree significantly with the values χ_{num} computed numerically, the estimated and computed values of short-time Lyapunov exponents for different orbit segments with the same energy should be strongly correlated. For example, chaotic segments for which the true short-time χ_{num} is especially small should yield estimates χ_{est} that are also especially small.

That such correlations do in fact exist is illustrated in FIGS. 13 (b) and (c) and FIG. 14, which exhibit results appropriate for, respectively, the truncated Toda and dihedral potentials. Each of these FIGURES was generated by (i) selecting a representative ensemble of 1000 initial conditions, all with the same energy; (ii) evolving these into the future for a time $T = 1024$ while simultaneously tracking the evolution of a small perturbation so as to generate χ_{num}; (iii) recording the values of K for each orbit at fixed intervals $\delta t = 0.4$; (iv) analyzing each orbit to extract $\langle K \rangle$ and δK; and (v) using these two moments along with Eq.(4.13) to generate an estimated χ_{est}. The scatter plots provide unambiguous visual confirmation that the values of χ_{num} and χ_{est} are strongly related.

This visual impression can be quantified by computing the Spearman rank correlation $\mathcal{R}$ between the values of χ_{est} and χ_{num} in each ensemble, which satisfies

$$\mathcal{R}(\chi_{num}, \chi_{est}) = 1 - \frac{6}{N^3 - N} \sum_{i=1}^{N} \delta_i^2. \qquad (6.1)$$

Here $N = 1000$ denotes the number of orbits in the ensemble and δ_i denotes the difference in rank for the ith orbit when ordered in terms of χ_{num} and χ_{est}. $\mathcal{R} = 1$ corresponds to a perfect correlation; $\mathcal{R} = -1.0$ corresponds to a complete anti-correlation.

The data sets in FIG. 13 (b) and (c), corresponding to $E = 30$ and $E = 50$ in the truncated Toda potential, both yield $\mathcal{R} \approx 0.88$. The data sets in FIG. 14 (a) - (e), corresponding to $E = 1.0$ in the dihedral potential, yield rank correlations ranging between a low of $\mathcal{R} \approx 0.85$ for $D = 3$ and a high of $\mathcal{R} \approx 0.95$ for $D = 2$. The especially high rank correlation for $D = 2$ might seem surprising since the ensemble contains a large number of regular orbit segments, with very small χ_{num}. The reason $\mathcal{R}$ remains as large as it does is that, for orbit segments that are manifestly regular, so the χ_{num} eventually decays to zero, there is a correlation between the estimated value χ_{est} and the rate at which χ_{num} tends to zero: for regular orbits where the short-time χ_{est} is especially large, the convergence is especially slow, so that, at finite times, χ_{num} will also be especially large [18].

Not surprisingly, the computed value of $\mathcal{R}$ for a given ensemble of initial conditions depends on the total in-

tegration time. If the orbits be integrated for a sufficiently large T, their differences tend to 'wash out,' so that the observed range of values for χ_{num} and χ_{est} both decrease. Eventually, the differences between different orbit segments become small and the pronounced correlation disappears.

It would seem visually from FIG. 14 (a) - (e) that the numerical and estimated values of the short-time Lyapunov exponents deviate largely because of some overall scaling. Given that at least for $D \geq 3$, the phase space is almost entirely chaotic, so that the distribution of curvatures reflects a microcanonical distribution, the evidence (cf. FIG. 6) that this implies a nearly Gaussian distribution, and the argument in the preceding subsection that quasi-isotropy is not necessarily the principal source of discrepancies, it would seem natural to conjecture that this reflects a misidentification of the proper autocorrelation time τ. Panel (f) in FIG. 14 shows what happens to the estimated value χ_{est} for the $D = 6$ dihedral potential if, for each orbit, τ is reduced by a factor of ≈ 0.75, the value required to ensure that, for the ensemble, the mean values of the estimated and numerical exponents coincide, *i.e.,* $\langle \chi_{num} \rangle = \langle \chi_{num} \rangle$. The net result is that, to a fair degree of approximation, the data points are aligned along $\chi_{est} = \chi_{num}$.

C. The special case $D = 2$

It is natural to ask whether one can relax the assumption of quasi-isotropy, at least for $D = 2$ where it would seem most suspect. One way in which to do this would be to work instead with the Jacobi metric, which, for $D = 2$, leads to a single oscillator equation of the form [7] [19]

$$\frac{d^2\xi}{dt^2} - \frac{1}{W}\frac{dW}{dt}\frac{d\xi}{dt} + \tilde{K}\xi = 0, \tag{6.2}$$

where $W = E - V(q^i)$ denotes the kinetic energy and

$$\tilde{K} = \Delta V + \frac{1}{W}|\nabla V|^2. \tag{6.3}$$

Unfortunately, however, this equation is very difficult to explore numerically since it yields near-divergences for $W \approx 0$, which prove quite common for $D = 2$.

Alternatively, within the setting discussed hitherto in this paper, there are two ways in which one might proceed:

1. Consider the full multi-dimensional Jacobi equation and view it as a matrix stochastic equation. This could at least provide the 'average' rate of exponential instability in different configuration space directions. Quite generally, a small perturbation ξ^i will satisfy

$$\frac{d^2\xi^i}{dt^2} + \sum_j V_{ij}\xi^j = 0, \tag{6.4}$$

with $V_{ij} \equiv \partial^2 V/\partial q^i \partial q^j$ the second derivative matrix. The objective then is to view each component of this matrix as an (approximately) independent stochastic variable, *i.e.,* considering

$$V_{ij} = V_{ji} = \Omega_{0,ij} + \delta\Omega_{ij}, \tag{6.5}$$

with $\delta\Omega_{ij}$ a random variable. Given distributions $N[V_{xx}]$, $N[V_{yy}]$, and $N[V_{xy}] = N[V_{yx}]$, which can be computed from time-series data or assuming ergodicity, and some approximation to the autocorrelation functions Γ_{xx}, Γ_{yy}, and Γ_{xy}, which can again be motivated either from a time series or assuming ergodicity, this system is easy to solve numerically. [20]

2. At least for $D = 2$, it is easy to diagonalise the matrix equation (4.2) at any given instant so as to obtain the eigenvalues of the stability matrix. The corresponding eigenvectors will then satisfy equations of the form

$$\frac{d^2\xi_\pm}{dt^2} + \omega_\pm \xi_\pm = 0, \tag{6.6}$$

where the time-independent eigenvalues satisfy

$$\omega_\pm = \frac{1}{2}\left(V_{xx} + V_{yy}\right) \pm \frac{1}{2}\left[\left(V_{xx} - V_{yy}\right)^2 + 4V_{xy}^2\right]^{1/2}. \tag{6.7}$$

Viewing $\omega_\pm = \Omega_{0,\pm} + \delta\Omega_\pm$ as stochastic variables leads to a pair of decoupled oscillator equations which are easy to solve numerically. In general, one might anticipate that the smaller eigenvalue will correspond to the more rapid growth rate.

These alternative were tested in detail for the $D = 2$ dihedral potential. The principal results are summarised in FIG. 10, which shows the numerical $\chi_{num}(E)$ (solid line) as well as estimated values $\chi_{est}(E)$ generated in four different ways. The short and long dashed lines, discussed already in the preceding section, correspond to the isotropized equation (4.9), assuming a microcanonical distribution (short dashes) or using inputs generated from orbital data (long dashes). The triple-dot dashed curve represents the values generated for the coupled oscillator system and the dot dashed curve represents the values generated by solving Eq. (6.6) for ω_-. All the estimated curves yield values χ_{est} that agree with χ_{num} to within factor of two, but none seems especially better than the others.

The hypothesis that chaotic behavior in lower-dimensional Hamiltonian systems can be modeled by a stochastic-oscillator equation would appear robust in the sense that different implementations all lead to predictions that yield at least rough agreement with numerical integrations. However, none of the alternatives considered here would appear 'completely right.' It seems likely that, in very low-dimensional systems, the details matter sufficiently that no universal prescription will yield a completely accurate prediction.

VII. CONCLUSIONS AND DISCUSSION

The results described in this paper strongly corroborate the intuition that chaotic motion in lower-dimensional Hamiltonian systems can be visualized as random, so that the average instability of chaotic orbits, and hence the values of their largest Lyapunov exponents, can be derived from a harmonic oscillator equation with a randomly varying frequency. Modulo straightforward modifications, technical rather than conceptual in nature, the approach introduced by Casetti *et al.* for higher-dimensional systems also works reasonably well for systems with dimensionality as low as $D = 2$. In this sense, as suggested in the Introduction, one would appear to have a clear new paradigm in terms of which to interpret the origins of chaos in lower-dimensional Hamiltonian systems.

The precise numerical values of χ predicted using this analytic approach are somewhat less accurate in lower dimensions than they are for much larger D, but it remains true that, in general, this approach yields predictions that are correct to within factors of two. In principle one might hope to do still better but, as a practical matter, this would seem difficult if not impossible. The 'obvious' alternatives considered in Section VI C yield somewhat different predictions for the largest Lyapunov exponents. In some cases these predictions are somewhat better than those based on Eqs. (4.12), (4.15), and (4.16) but, overall, they seem neither appreciably better nor appreciably worse. This would suggest that the predictions based on these equations are comparatively robust, in the sense that minor modifications do not yield vastly different results. However, this might also suggest that there is no single, universal modification that one might introduce which would yield near-perfect agreement for all potentials and energies. In point of fact, this is hardly surprising. There is every reason to expect that details which should 'wash out' in higher-dimensional systems will remain important in lower-dimensional systems. A 'thermodynamic' description of chaos should work best for systems with many degrees of freedom.

In this context, two significant points should be stressed.

(1) Even when the predicted values $\chi_{est}(E)$ of the 'true' Lyapunov exponent $\chi_{num}(E)$ are off by as much as factors of two, one observes strong correlations between $\chi_{est}(E)$ and $\chi_{num}(E)$ for different orbit segments with the same energy. Orbit segments for which the predicted χ_{est} is low tend to have small short-time exponents χ_{num}; and, similarly, segments for which χ_{est} is high tend to have larger values of χ_{num}. The physics entering into Eqs. (4.12), (4.15), and (4.16) allows one to distinguish clearly between orbit segments that are 'wildly chaotic' in visual appearance and have especially large short-time exponents and 'sticky' segments that are nearly regular in appearance and have comparatively small short-time exponents.

(2) The largest discrepancies between the predicted and numerically computed Lyapunov exponents occur invariably for those potentials and energies where large portions of the chaotic sea correspond to 'sticky' orbits manifesting nearly regular behavior, in which case χ_{est} can be much larger than the 'true' χ_{num}. This is exactly what one would expect. If large portions of the stochastic sea are 'sticky,' an orbit will spend much of its time evolving in a nearly regular fashion, but it is clear that, while manifesting such near-regular behavior, its motion cannot be characterised as essentially random. Indeed, as discussed more carefully elsewhere [7], chaotic orbit segments for which $\langle K \rangle$ and δK assume values close to those characteristic of regular orbits tend systematically to have very small short-time Lyapunov exponents.

The principal difference between the approach developed in this paper and the approach introduced by Casetti *et al.* is that the statistical properties of the mean curvature K are not derived assuming a canonical distribution. For a truly conservative system, a thermodynamic description must, strictly speaking, be based on a microcanonical distribution, and it is only for large D that one can approximate such a 'correct' description by a description based on a canonical distribution. Moreover, for very low dimensions, especially $D = 2$, even a microcanonical distribution is clearly unjustified. A microcanonical analysis is based on the assumption that the entire constant-energy hypersurface is chaotic, but for lower dimensions, non-integrable systems typically exhibit a coexistence of regular and chaotic regions, both with significant measure. A correct analysis must involve deriving the statistics of the curvature only in the chaotic phase-space regions, a task which seems difficult analytically but, given an assumption of ergodicity, is straightforward to implement via a time-series analysis.

In part, this work concerning chaos and the phase mixing of chaotic orbits was motivated in the context of nonequilibrium systems comprised of a large number of interacting particles. Examples of such systems include self-gravitating systems, *e.g.*, galaxies, and charged-particle beams governed by external focusing forces and internal Coulomb forces (space charge). For both these examples fast evolutionary time scales have profound consequences. For galaxies, they are an integral part of the formation process [21]. For beams, they limit the degree to which an accelerator designer can preserve the beam quality, especially insofar as the evolution is irreversible [22].

As mentioned in Section II, one way to infer the fastest time scale is to consider the interaction of a single particle with the coarse-grained potential formed by all the other particles. The problem then reduces to one involving a low-dimensional Hamiltonian, and the obvious question is to what extent statistical arguments concerning the behavior of chaotic single-particle orbits can be invoked to simplify the analysis further. All the examples presented herein suggest that time scales in low-dimensional Hamiltonian systems inferred via the statistical methods

of Casetti *et al.* are typically valid within a factor of order two. They also suggest that uncertainties in the computation of these time scales are principally associated with uncertainties in the autocorrelation time, and that these time scales are comparatively insensitive to the choice of the invariant measure that weights the statistical averages. More importantly, however, our examples reinforce the idea advanced by Cerruti-Sola and Pettini [23] that rapid mixing originates from parametric instability due to positive-curvature fluctuations along the geodesic trajectories of the particles over the configuration-space manifold. Cerruti-Sola and Pettini conjectured that: "This mechanism is apparently the most relevant – and in many cases unique – source of chaoticity in physically meaningful Hamiltonians." The diverse set of examples presented here would seem to corroborate their conjecture.

The statistical analysis, however, does carry some *caveats*. It generally 'predicts' fast exponential mixing in potentials that are known *a priori* to be integrable and thereby admit only regular orbits that can only mix secularly. Examples include spherically symmetric potentials for which Poisson's equation generates nonuniform density distributions, and special triaxial potentials such as the Staeckel potentials [24]. Thus the analysis provides no information as to what criteria are necessary and sufficient to establish a preponderance of globally chaotic orbits; it merely hypothesizes their existence. Related to this deficiency is the failure of the analysis to account for 'sticky' chaotic orbit segments that, when present, will tend to slow down the mixing. Real systems may, however, mitigate these *caveats*. For example, external noise, even with very small amplitude, is known to add greatly to the efficiency of chaotic mixing by overcoming 'stickiness' [25]. And the presence of localized irregularities that have been coarse-grained away may increase the chaoticity of the orbits. An important point, however, is that graininess which manifests itself in binary particle interactions is *not* an example of such localized irregularities. Graininess establishes diffusion of an orbit away from the trajectory it would have in the smooth potential but, at least for nonchaotic orbits, this diffusion involves a secular, rather than exponential, divergence of trajectories [26].

Because it is based on the Eisenhart metric, the present treatment is restricted to stationary systems. However, with a Finsler metric, the geometric method can also incorporate potentials that are explicitly time-dependent and/or velocity-dependent [27]. For example, recent work involving the Hénon-Heiles potential [28] resulted in a geometric measure of chaos over the associated Finsler manifold that was used for fast computation of the system's Poincaré surface of section. If used with a coarse-grained potential, the Eisenhart metric includes no mechanism for changing the particle energies. In principle, it can be included with a Finsler metric based on a time-dependent coarse-grained potential; however, the generalization also requires specifying a suitable invariant measure for the nonequilibrium system [29].

One final point should be noted. In writing this paper, the authors have deliberately adopted a tact somewhat complementary to that adopted by Casetti *et al.* Rather than focusing on the differential geometry of spaces admitting an Eisenhart metric, the discussion has, to the extent possible, been couched in the language of conventional Hamiltonian mechanics. Such an approach serves to make the physical ideas underlying the general approach more transparent physically and, it is hoped, will make the picture of chaotic motion as a random process comprehensible to a substantially larger audience.

ACKNOWLEDGMENTS

This research was supported in part by NSF AST-0070809, and in part by the Universities Research Association, Inc., under contract DE-AC02-76CH00300 with the U.S. Department of Energy.

---

[1] See, e.g., A. J. Lichtenberg and M. A. Lieberman, *Regular and Chaotic Dynamics* (Springer: Berlin, 1992).
[2] L. P. Eisenhart, Ann. Math. **30**, 591 (1929).
[3] E. Hopf, Trans. Am. Math. Soc. **39**, 229 (1936)
[4] D. V. Anosov, Trudy Mat. Inst. Steklov **90**, 1 (1967).
[5] M. Pettini, Phys. Rev. E **47**, 828 (1993).
[6] M. Toda, J. Phys. Soc. Jap. **22**, 431 (1967).
[7] H. E. Kandrup, Phys. Rev. E **56**, 2722 (1997).
[8] L. Casetti, C. Clementi, M. Pettini, Phys. Rev. E **54**, 5969 (1996).
[9] H. E. Kandrup and I. V. Sideris, Celestial Mechanics, in press (2001).
[10] D. Armbruster, J. Guckenheimer, S. Kim, Phys. Lett. **A 140**, 416 (1989).
[11] Cf. J. Ford, Phys. Rep. **213**, 271 (1992).
[12] Cf. P. Grassberger, P. Badii, A. Poloti, J. Stat. Phys. **51**, 135 (1988).
[13] Cf. Section 44 of L. D. Landau and E. M. Lifshitz, *Mechanics* (Pergamon: Oxford, 1969)
[14] N. G. Van Kampen, Phys. Rep. **24**, 71 (1976).
[15] G. Contopoulos, Astrophys. J. **76**, 147 (1971).
[16] Cf. I. V. Pogorelov and H. E. Kandrup, Phys. Rev. E **60**, 1567 (1999). Fig. 1 in that paper exhibits examples of 'sticky' orbits in the potentials (3.1) and (3.2).
[17] Recall that, at least for a Gaussian distribution, the form of Γ is known to be irrelevant: any Γ that yields the correct autocorrelation time will yield the same estimated χ_{est}.
[18] Correlations between curvature and the rate of convergence for regular orbits are implicit in, *e.g.,* FIGS. 3 - 5 of Ref. 7.
[19] Eq. (23) in M. Cerruti-Sola and M. Pettini, Phys. Rev. E **53**, 179 (1996).

(b)

[20] Unfortunately, an analytic solution using the approach discussed in Section IV seems impossible. For a single oscillator equation, one is led to three coupled moment equations and, hence, a cubic equation for χ. For two coupled oscillators, one has eight coupled equations and, hence, an eighth order equation for χ.

[21] H. E. Kandrup, Astrophys. J. **500**, 120 (1998).

[22] C. L. Bohn, in *The Physics of High Brightness Beams*, edited by J. Rosenzweig and L. Serafini (World Scientific, Singapore, 2000), pp. 358-368.

[23] M. Cerruti-Sola and M. Pettini, *op. cit.*

[24] T. deZeeuw, Mon. Not. R. Astron. Soc. **216**, 273 (1985).

[25] C. Siopis and H. E. Kandrup, Mon. Not. R. Astron. Soc. **319**, 43 (2000).

[26] H. E. Kandrup and I. V. Sideris, Phys. Rev. E (submitted). Discreteness effects in a chaotic potential, modeled as friction and noise, typically trigger an exponential divergence.

[27] M. Di Bari, D. Boccaletti, P. Cipriani, and G. Puccaco, Phys. Rev. E **55**, 6448 (1997).

[28] P. Cipriani and M. Di Bari, Phys. Rev. Lett. **81**, 5532 (1998).

[29] G. Gallavotti, J. Math. Phys. **41**, 4061 (2000).

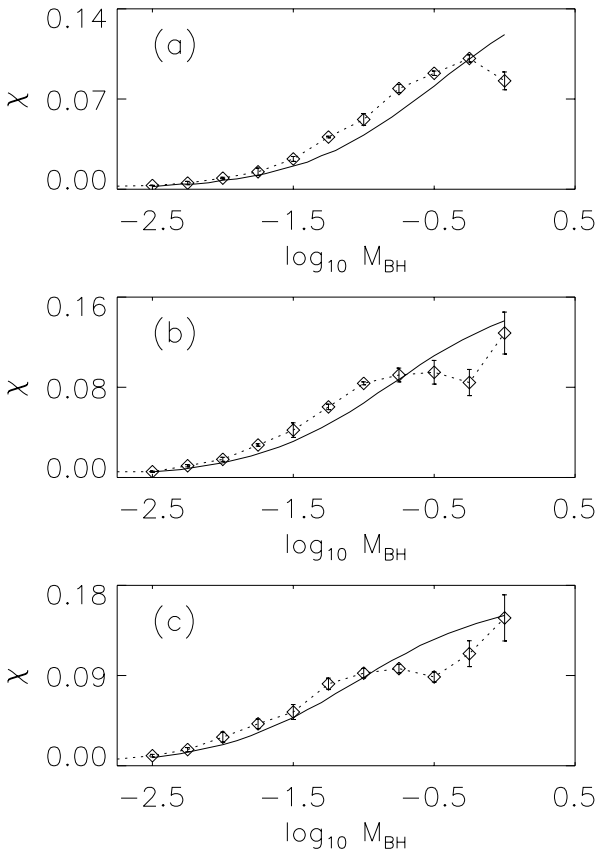

FIG. 1. (a) Numerical (diamonds) and analytic (solid line) estimates of the largest Lyapunov exponent for chaotic orbits evolved in the 3-dimensional galactic potential (2.1) with $a^2 = 0.75$, $b^2 = 1.0$, and $c^2 = 1.25$ as a function of black hole mass M_{BH} for total particle energy $E = 1.0$. (b) The same for $E = 0.6$. (c) $E = 0.4$.

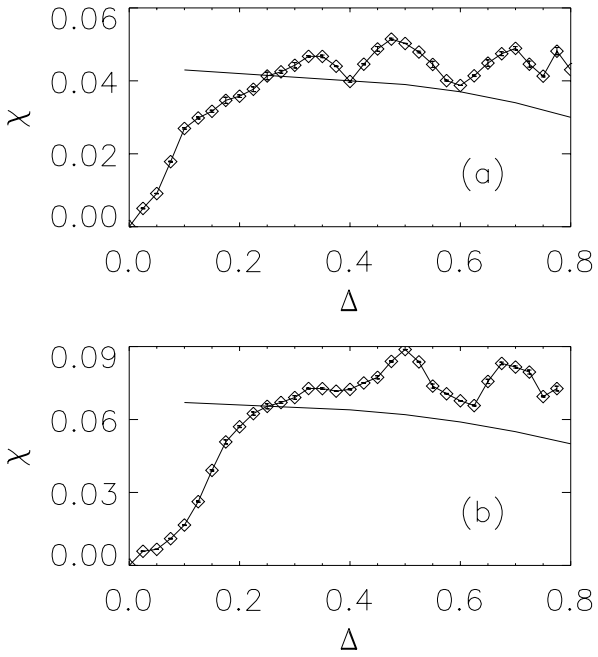

FIG. 2. (a) Numerical (diamonds) and analytic (solid line) estimates of the largest Lyapunov exponent for chaotic orbits evolved in the 3-dimensional galactic potential (2.1) ith $M_{BH} = 0.1$ and $a^2 = 1 - \Delta$, $b^2 = 1$, $c^2 = 1 + \Delta$ as a function of Δ for total particle energy $E = 1.0$. (b) The same for $E = 0.6$.

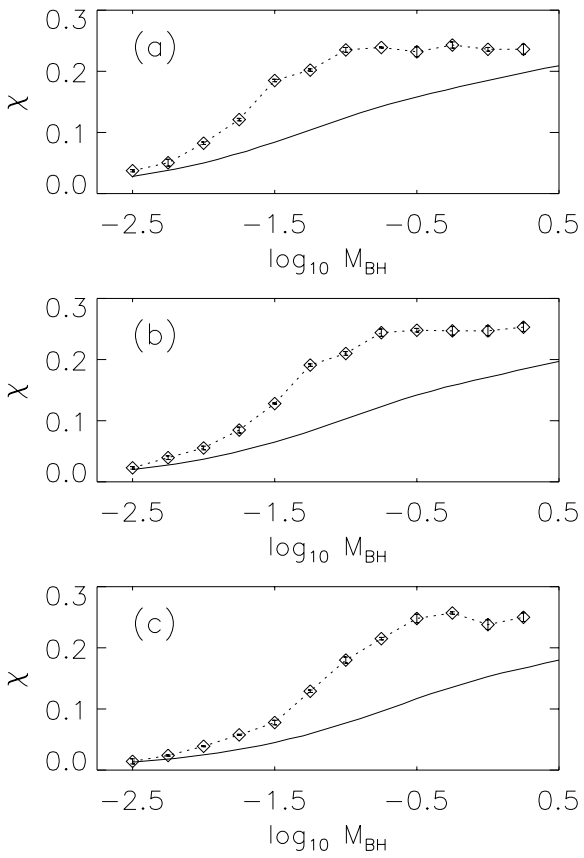

FIG. 3. Same as Fig. 1, but with all orbits restricted to the 2-dimensional (x, y)-plane.

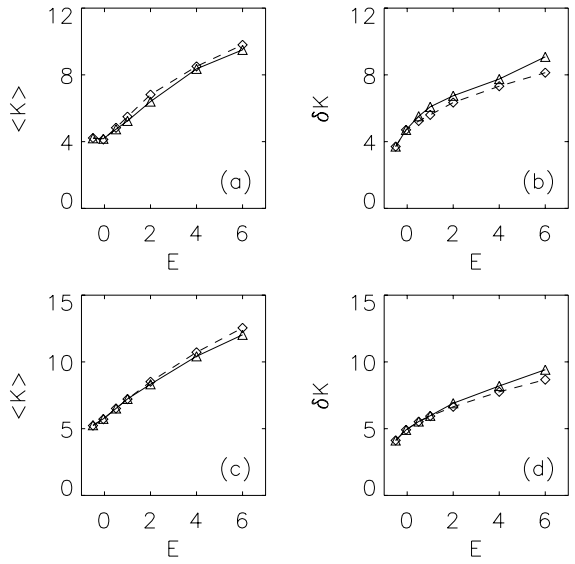

FIG. 4. (a) The mean curvature $\langle K \rangle$ for chaotic orbits in the $D = 2$ dihedral potential as a function of energy E, computed assuming a microcanonical distribution (solid line) and extracted directly from orbital data (dashed line). (b) The associated dispersion δK. (c) $\langle K \rangle$ for $D = 3$. (d) δK for $D = 3$.

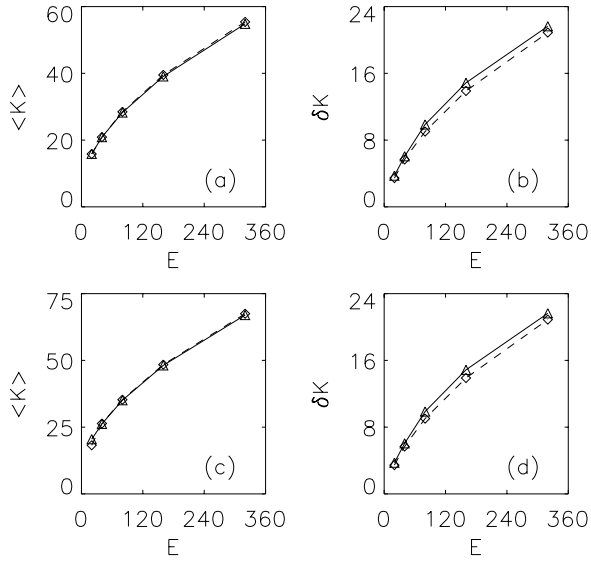

FIG. 5. (a) The mean curvature $\langle K \rangle$ for chaotic orbits in the $D = 4$ *FPU* potential with $a = 1.0$ and $b = 0.1$ as a function of energy E, computed assuming a microcanonical distribution (solid line) and extracted directly from orbital data (dashed line). (b) The associated dispersion δK. (c) $\langle K \rangle$ for $D = 6$. (d) δK for $D = 6$.

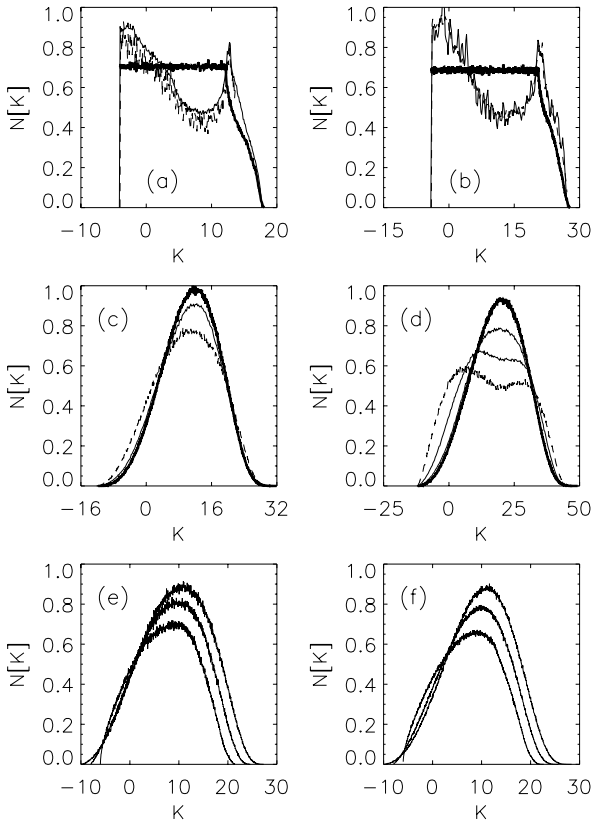

FIG. 6. (a) The distribution of curvatures, $N[K]$, for chaotic orbits with energy $E = 1.0$ in the $D = 2$ dihedral potential, computed assuming a microcanonical distribution (thick solid line) and from orbital data for an ensemble evolved for times $t = 1024$ and $t = 3172$. (b) $N[K]$ for $D = 2$ and $E = 6.0$. (c) $N[K]$ for $D = 6$ and $E = 1.0$. (d) $N[K]$ for $D = 6$ and $E = 6.0$. (e) $N[K]$, as generated from time-series data for $t = 3172$, for $E = 1.0$ with $D = 3$, $D = 4$, and $D = 5$. (f) $N[K]$ for $E = 1.0$ with $D = 3$, $D = 4$, and $D = 5$, now generated assuming a microcanonical distribution.

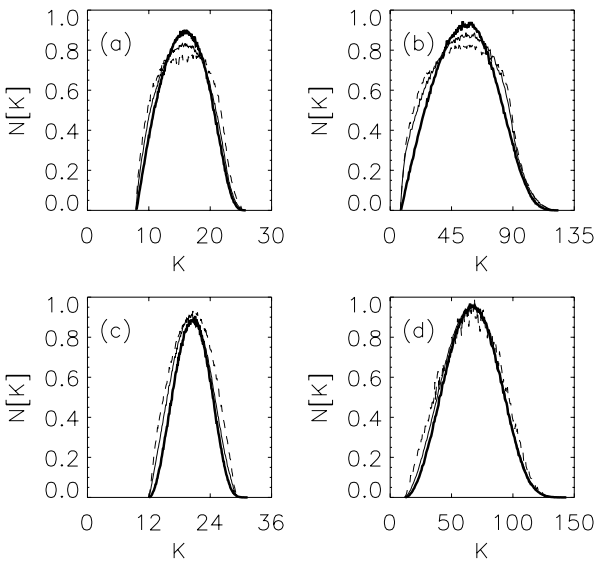

FIG. 7. (a) The distribution of curvatures, $N[K]$, for chaotic orbits with energy $E = 20$ in the $D = 4$ FPU potential with $a = 1.0$ and $b = 0.1$, computed assuming a microcanonical distribution (thick solid line) and from orbital data for an ensemble evolved for times $t = 1024$ and $t = 4196$. (b) $N[K]$ for $D = 4$ and $E = 320$. (c) $N[K]$ for $D = 6$ and $E = 20$. (d) $N[K]$ for $D = 6$ and $E = 320$.

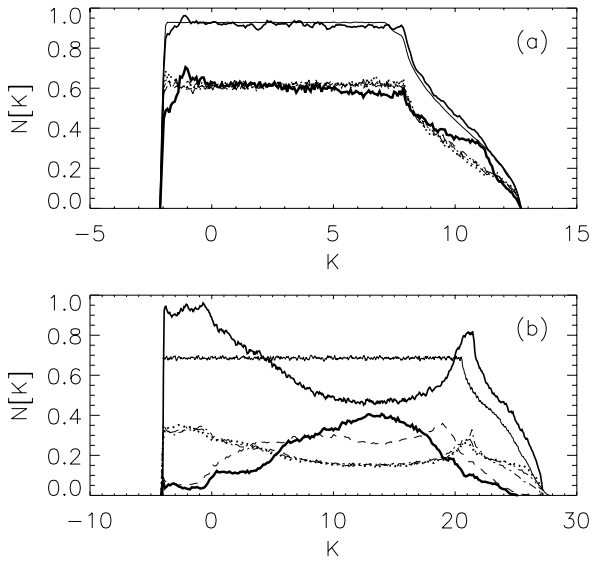

FIG. 8. (a) The distribution of curvatures, $N[K]$, for a representative ensemble of 1000 orbits with energy $E = -0.5$ in the $D = 2$ dihedral potential. The five lower curves represent subdistributions, generated by dividing the ensemble into five quintiles based on the values of the short-time Lyapunov exponents for the orbits. The near-horizontal upper curve represents the distribution $N[K]$ predicted by a microcanonical distribution; the other, more jagged upper curve represents the distribution $N[K]$ associated with the full 1000 orbit ensemble, given by the sum of the five lower curves. (b) The same for $E = 6.0$.

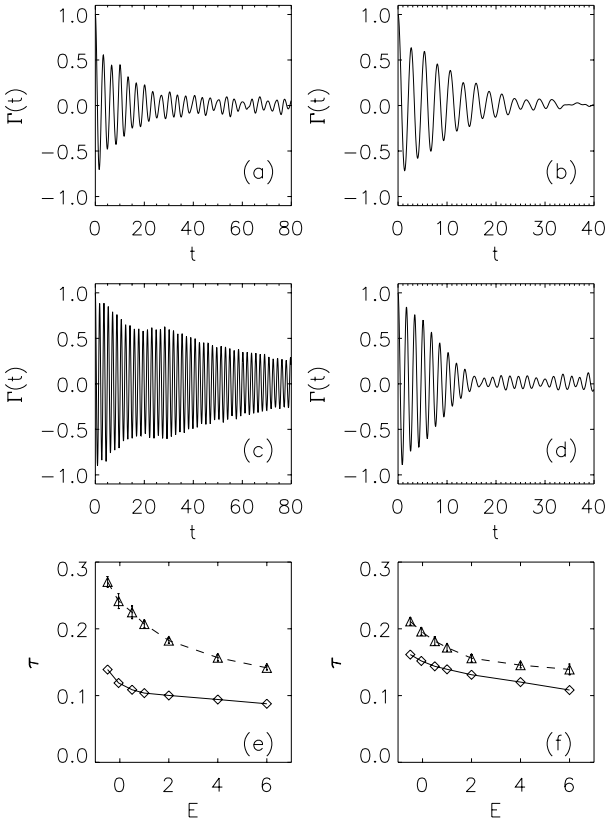

FIG. 9. (a) The autocorrelation function $\Gamma(t)$ for chaotic orbits in the $D = 2$ dihedral potential with $E = -0.5$. (b) The same for $D = 6$ and $E = -0.5$. (c) The same for $D = 2$ and $E = 6.0$. (c) The same for $D = 6$ and $E = 6.0$. (e) The Casetti*et al.* time scale τ of Eq. (4.12) (solid line) and the time scale $\tau_{osc}/4\pi$ of Eq. (4.14) (dashed line), for chaotic orbits in the $D = 2$ dihedral potential at different energies E. (f) The same for $D = 6$.

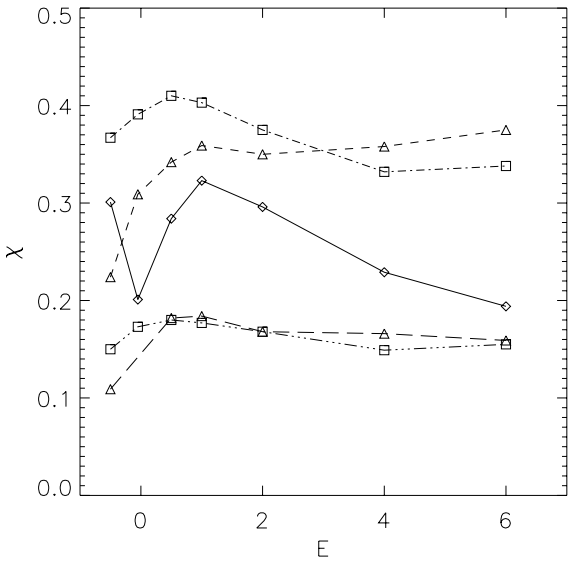

FIG. 10. Estimated values of the largest Lyapunov exponent for the $D = 2$ dihedral potential as a function of energy: χ_{num} generated from direct numerical integration (solid curve), the Casetti *et al.* value, generated assuming a Gaussian $N[K]$ and autocorrelation time τ given by Eq. (4.12) (short dashes); an estimate based on Eq. (4.8), but now using the $N[K]$ generated from a time-series analysis and τ given by Eq. (4.14) (long dashes); an estimate based on Eq. (6.6), using ω_- and τ given by Eq. (4.14) (dot-dashes); and an estimate based on the coupled oscillator system, assuming Gaussian fluctuations and τ given by Eq. (4.12).

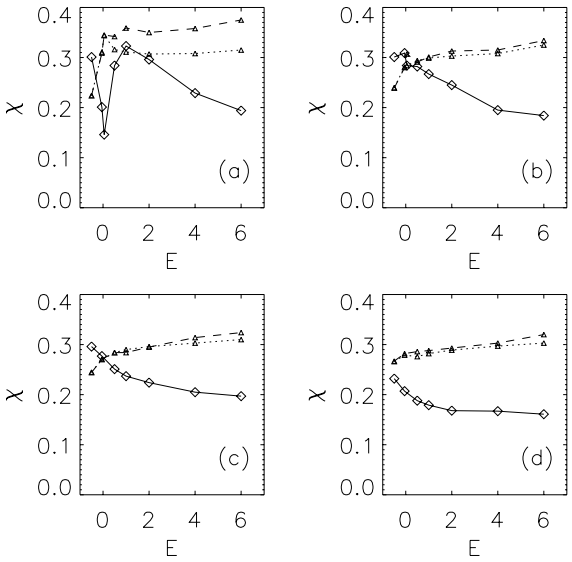

FIG. 11. Estimated values of Lyapunov exponents for orbits in the dihedral potential, generated from numerical integrations (solid lines) and estimated using Eq. (4.12). (a) For $D = 2$. (b) $D = 3$. (c) $D = 4$. (d) $D = 6$.

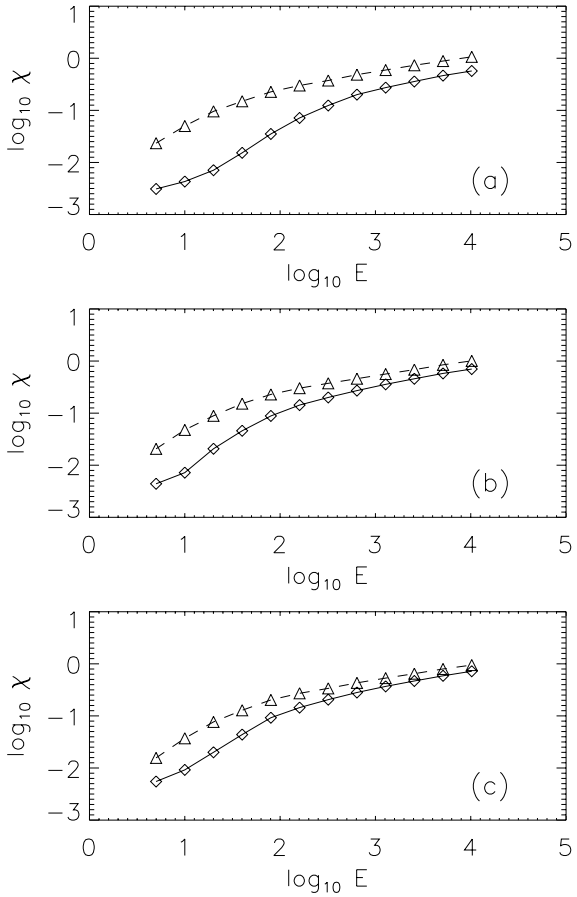

FIG. 12. Estimated values of Lyapunov exponents for orbits in the *FPU* model, generated from numerical integrations (solid lines) and estimated using Eq. (4.12). (a) For $D = 4$. (b) $D = 5$. (c) $D = 6$.

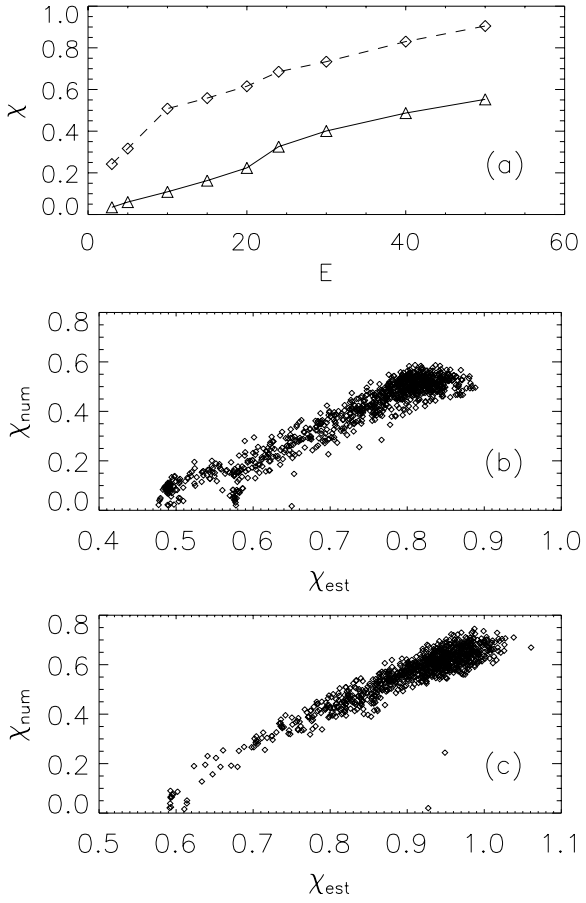

FIG. 13. (a) Estimated values of Lyapunov exponents for orbits in the truncated Toda potential, generated from numerical integrations (solid lines) and estimated using Eq. (4.12) (b) Short-time lyapunov exponents computed using Eq. (4.12) (χ_{est}) and generated from numerical integrations (χ_{num}) for $E = 30.0$. (c) The same for $E = 50.0$.

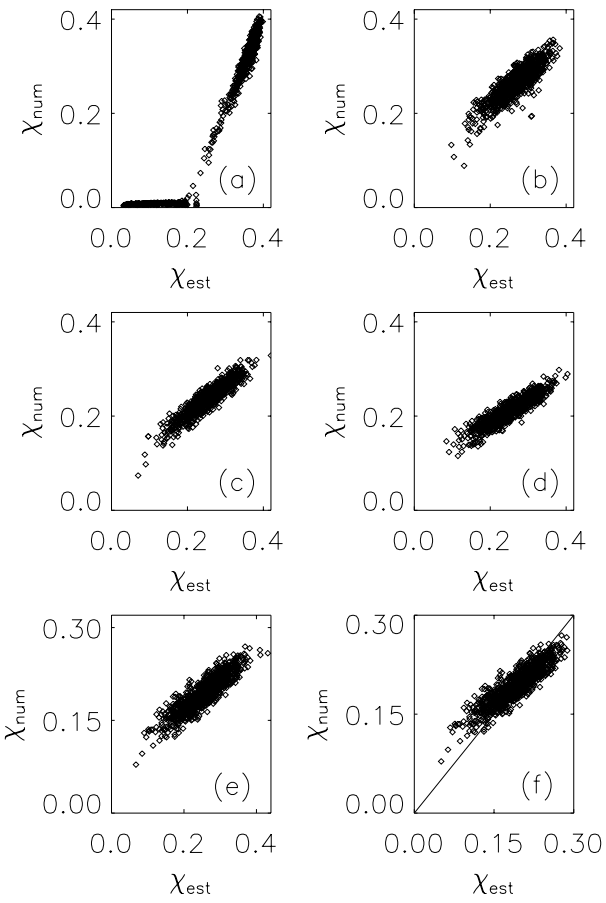

FIG. 14. (a) Short-time lyapunov exponents computed using Eq. (4.12) (χ_{est}) and generated from numerical integrations (χ_{num}) for $E = 1.0$ in the $D = 2$ dihedral potential. (b) The same for $D = 3$. (c) $D = 4$. (d) $D = 5$. (e) $D = 6$. (f) χ_{num} for $D = 6$ contrasted with revised estimates χ_{est} generated by rescaling the time scale τ of Eq. (4.12) by a factor of 0.75.